Crystal structure of Spot 14, a modulator of fatty acid synthesis

Christopher L. Colbert[a,1,2], Chai-Wan Kim[b,1], Young-Ah Moon[b], Lisa Henry[a,c], Maya Palnitkar[a,c], William B. McKean[b], Kevin Fitzgerald[d], Johann Deisenhofer[a,c,3], Jay D. Horton[b,e,3], and Hyock Joo Kwon[a]

[a]Department of Biochemistry and [b]Molecular Genetics, [c]Howard Hughes Medical Institute, and [e]Department of Internal Medicine, University of Texas Southwestern Medical Center, Dallas, TX 75390-9050; and [d]Alnylam Pharmaceuticals, 300 Third Street, Cambridge, MA 02142

Contributed by Johann Deisenhofer, August 26, 2010 (sent for review July 30, 2010)

Spot 14 (S14) is a protein that is abundantly expressed in lipogenic tissues and is regulated in a manner similar to other enzymes involved in fatty acid synthesis. Deletion of S14 in mice decreased lipid synthesis in lactating mammary tissue, but the mechanism of S14's action is unknown. Here we present the crystal structure of S14 to 2.65 Å and biochemical data showing that S14 can form heterodimers with MIG12. MIG12 modulates fatty acid synthesis by inducing the polymerization and activity of acetyl-CoA carboxylase, the first committed enzymatic reaction in the fatty acid synthesis pathway. Coexpression of S14 and MIG12 leads to heterodimers and reduced acetyl-CoA carboxylase polymerization and activity. The structure of S14 suggests a mechanism whereby heterodimer formation with MIG12 attenuates the ability of MIG12 to activate ACC.

lipogenesis | posttranslational | regulation

Fatty acid synthesis is a tightly regulated process that occurs at multiple levels within the cell. This regulation is essential for normal cellular function because fatty acids are required for phospholipid synthesis, triglyceride formation, and to serve as signaling molecules; however, excess fatty acid accumulation in cells can contribute to the pathogenesis of fatty liver disease, diabetes, cancer, and obesity (1, 2). The synthesis of fatty acids up to 16 carbons in length requires the action of only three enzymes, ATP citrate lyase, acetyl-CoA carboxylase (ACC), and fatty acid synthase. The most highly regulated of the three enzymes is ACC, the first committed enzyme in fatty acid synthesis.

ACC catalyzes the carboxylation of acetyl-CoA to malonyl-CoA, the rate-limiting and first committed step in de novo fatty acid biosynthesis. Two isoforms of ACC exist in mammals, ACC1 and ACC2, and both enzymes function to carboxylate acetyl-CoA to form malonyl-CoA (3–5). Mammalian ACCs are dimeric, multifunctional enzymes composed of four distinct domains: a biotin carboxylase (BC) domain, a biotin carboxyl carrier protein (BCCP) domain, the ACC central region, and a carboxyltransferase (CT) domain. Structures of the isolated BC (6–8), BCCP (9), and CT (10, 11) domains from various organisms show that the BC domain exists in both monomeric and dimeric forms, the BCCP domain is a monomer, and the CT domain exists as a dimer. The regulation of ACCs occurs at multiple levels: transcriptional regulation via sterol regulatory element binding protein (SREBP), liver X receptor, and carbohydrate responsive element binding protein (ChREBP) (12–14), phosphorylation/dephosphorylation (15, 16), and allosteric activation by citrate, which induces polymerization and increases the activity of ACC (1).

Recently, we reported the discovery that MIG12, a 183 amino acid protein, binds to ACC1 and ACC2, which induces polymerization and subsequently increases the enzymatic activity of the protein (17). The overexpression of MIG12 in mice resulted in high rates of fatty acid synthesis in liver and in the development of hepatic steatosis (17). Thus, the regulation of ACC by MIG12 can have important physiological consequences.

The only protein in the GenBank database that shares significant homology with MIG12 is a protein designated Spot 14 (S14). S14 is a 150 amino acid protein that was initially discovered by Oppenheimer and colleagues (18) in a screen for proteins that were regulated by thyroid hormone in rat livers. Subsequent studies revealed that S14 is highly expressed in tissues with high rates of lipogenesis (19), and the gene is highly regulated at the transcriptional level by SREBP-1c (12, 20) and ChREBP (21), transcription factors that activate all genes involved in fatty acid synthesis (22). Although the molecular function of S14 is unknown, S14 knockout mice have reduced fatty acid synthesis in lactating mammary glands (23) but increased lipid synthesis in liver (24). However, in cultured rat primary hepatocytes, knockdown of both S14 and MIG12 using RNAi reduced fatty acid synthesis by ∼65% (25).

Although S14 and MIG12 share 32% identity, S14 does not bind and activate ACC (17), and the biochemical function of S14 remains unknown. In the current study, we have determined the crystal structure of mouse S14 to 2.65-Å resolution. The structure of S14 reveals a helical protein arranged as a symmetric dimer. Cultured cell experiments indicate that S14 can form heterodimers with MIG12, suggesting a mechanism through which S14 could modulate ACC activity and subsequently rates of fatty acid synthesis via heterodimer formation with MIG12.

Results

A recombinant form of mouse S14, spanning residues 1–150, was used for structural studies. S14 exists as a dimer in solution according to size exclusion chromatography and analytical ultracentrifugation (*SI Text*, Fig. S1). Recombinant S14 was unable to activate or induce polymerization of ACC1 (17).

Structure of S14. The structure of S14 was determined by single wavelength anomalous diffraction phasing and refined to 2.65 Å (Table 1). The model spans residues 8–149, although residues 46–48 and 77–104 are poorly ordered and were not placed in the electron density. S14 crystallized in the space group *I*432 with a single monomer in the asymmetric unit. The biologically relevant dimer can be constructed using crystallographic symmetry.

The main body of the S14 monomer is composed of three antiparallel α-helices (Fig. 1*A*). Helices 1 and 2 are ∼30 Å in length and helix 3 is ∼60 Å in length. The increased length of helix 3 allows it to interact with an adjacent monomer. There-

Author contributions: C.L.C., C.-W.K., Y.-A.M., J.D.H., and H.J.K. designed research; C.L.C., C.-W.K., L.H., M.P., W.B.M., and H.J.K. performed research; K.F. contributed new reagents/analytic tools; C.L.C., C.-W.K., Y.-A.M., J.D.H., and H.J.K. analyzed data; and C.L.C., C.-W.K., Y.-A.M., J.D., J.D.H., and H.J.K. wrote the paper.

The authors declare no conflict of interest.

Data deposition: The atomic coordinates and structure factors have been deposited in the Protein Data Bank, www.pdb.org (PDB ID code 3ONT).

[1]C.L.C. and C.-W.K. contributed equally to this work.

[2]Present address: Department of Chemistry and Biochemistry, North Dakota State University, Fargo, ND 58108-6050.

[3]To whom correspondence may be addressed. E-mail: johann.deisenhofer@utsouthwestern.edu or jay.horton@utsouthwestern.edu.

This article contains supporting information online at www.pnas.org/lookup/suppl/doi:10.1073/pnas.1012736107/-/DCSupplemental.

Table 1. Data collection and model refinement statistics

Data collection statistics	
Space group	*I*432
a, *b*, *c*, Å	144.9
Resolution, Å (final shell)	50–2.64 (2.69–2.64)
Reflections	
Total	261,643
Unique	7919
Completeness, %	99.8 (100.0)
Average multiplicity	9.1 (7.5)
R_{sym}*, %	6.3 (55.2)
Model refinement statistics	
Resolution, Å	39–2.65
No. of reflections	7512
R_{work}, %	22.3
R_{free}, %	24.9
rms deviations from target values	
Bond lengths, Å	0.013
Bond angles, °	1.39

Values in parentheses pertain to the outermost shell of data.
*$R_{sym} = \sum_{h,i}|I_{h,i} - \langle I_h\rangle|/\sum_{h,i}I_{h,i}$.

by, an antiparallel 4-helix bundle is created by packing the C terminus of helix 3 against the main body of the other monomer to form the homodimer (Fig. 1*B*). The S14 dimer is ~25 × 30 × 75 Å with the monomers related by 2-fold symmetry. The total surface area buried at the dimer interface is ~2,650 Å^2 with helix 3 burying ~1,400 Å^2 through its interaction with the neighboring monomer (Fig. 2*A*).

Sequence Conservation Between S14 and MIG12. Analysis of the sequence conservation between S14 and MIG12 revealed that the dimer interface of S14 is highly conserved between S14 and MIG12, whereas two regions of lowest conservation, termed box A and B, are not involved in dimerization (Fig. 2 *B* and *C*).

Interaction of S14 and MIG12 in Cultured Cells. To determine whether S14 directly interacted with MIG12, the proteins were overexpressed in Chinese hamster ovary-K1 (CHO-K1) cells (Fig. 3). In one set of experiments, S14 contained a FLAG tag and in the second set of experiments MIG12 contained a FLAG tag. Cell lysates were incubated with an anti-FLAG antibody to precipitate either S14 or MIG12, and supernatants and pellets were subjected to SDS-PAGE. S14, MIG12, and ACC1 were visualized by immunoblot analysis using antibodies that recognize ACC1,

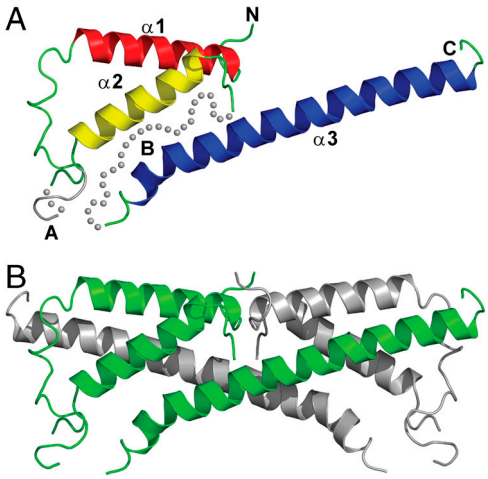

Fig. 1. Structure of S14. (*A*) The structure of the S14 monomer reveals three antiparallel α-helices. The regions of lowest homology to MIG12 (box A and B) are shown in gray. Disordered regions in the structure are indicated with spheres. (*B*) The S14 homodimer creates two antiparallel 4-helix bundles in a symmetric arrangement. Each monomer is colored either green or gray.

S14, and MIG12 as described in the *Materials and Methods*. As shown in Fig. 3, both S14 and MIG12 were able to coimmunoprecipate each other as well as ACC1, although the efficiency of ACC1 coimmunoprecipitation with S14 was markedly weaker than with MIG12 and likely represents S14's interaction with the MIG12:ACC complex.

To confirm that a direct interaction between S14 and MIG12 exists, we analyzed the interaction of S14 and MIG12 by Blue Native PAGE (Fig. 4*A*). Overexpression of either S14 or MIG12 alone in CHO-K1 cells resulted in the formation of homodimers of the overexpressed protein; however, the coexpression of MIG12 and S14 resulted in the formation of heterodimers in the cell (Fig. 4*A*). To determine whether the quantity of S14 changed the relative amounts of MIG12 that heterodimerized with S14, CHO-K1 cells were transfected with MIG12 and increasing amounts of S14 and cell lysate proteins were separated by Blue Native PAGE for immunoblot analysis. As shown in Fig. 4*B*, MIG12 incorporation into heterodimer complexes increased as a function of S14 concentration.

S14 Reduces the Activity of MIG12 in Cultured Cells. To determine if S14 altered the function of MIG12, we monitored the polymerization and ACC activity in the presence of MIG12 and increasing amounts of S14 (Fig. 5 *A* and *C*). Increasing S14 levels resulted in reduced ACC polymerization (Fig. 5*A*) and less MIG12 incorporation into ACC polymers (Fig. 5*B*). Consistent with the reduced polymerization of ACC, the activation of partially purified ACC also decreased with increasing levels of S14 (Fig. 5*C*).

S14 Knockdown Increases ACC Polymerization and Activity in Vivo. To determine whether S14 participates in the regulation of ACC in vivo, we knocked down S14 in livers of living mice by injecting S14 oligos or S14 oligos containing a mismatch (MM) formulated into lipidoid nanoparticles (Fig. 6). One week after injection of S14 siRNA into mice, livers were harvested using a freeze clamp technique. Cytosolic proteins prepared from livers were analyzed by Blue Native PAGE, and immunoblot analysis was carried out for S14 and MIG12. The siRNA directed against S14 reduced the mRNA levels of S14 by ~90% and the S14 protein was below the detection limits of the antibody (Fig. 6*A*). In mice injected with a control MM siRNA, MIG12 was present primarily as a heterodimer with S14. In contrast, most S14 normally is present as a homodimer based on the sizes of the complexes in the Blue Native PAGE. Reduction of S14 by siRNA knockdown resulted in the formation of MIG12 homodimers (Fig. S2), which resulted in increased MIG12-induced ACC1 polymerization and activity (Fig. 6 *B* and *C*). In a separate study, male mice were injected with the S14 siRNA and after 5 d they were injected with tritiated water to measure in vivo rates of hepatic fatty synthesis. As shown in Fig. 6*D*, the knockdown of S14 resulted in a 30% reduction in rates of hepatic fatty acid synthesis.

Discussion

The structure of S14 reveals that it exists as a homodimer, and analysis of the residues involved in dimerization reveals that the dimer interface is conserved or highly similar between S14 and MIG12 (Fig. 2*C*). Helix 3 is unable to dimerize in isolation, and dimerization requires helix 3 from one monomer and helix 1 and 2 from another (26, 27). This is consistent with the crystal structure of S14 where the C terminus of helix 3 packs against helix 1 and 2 of the other monomer and is the major region of interaction within the dimer. Sequence conservation between S14 and MIG12 is highest across helix 3 (50% overall identity and 57% identity for residues at the dimer interface). Nonconserved residues in MIG12 at the dimer interface either pack against conserved residues or are solvent accessible (Fig. 2*B*). Conservation of the dimer interface in S14 and MIG12 suggested that S14 and MIG12 form heterodimers. The coimmunoprecipitation and

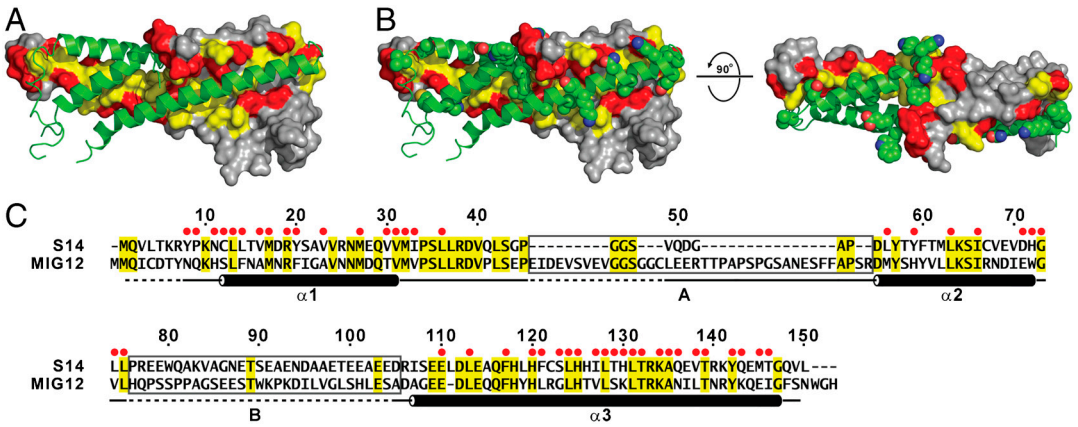

Fig. 2. The S14 dimer interface. (*A*) The buried surface of a S14 monomer within the S14 homodimer is shown in red (nonconserved residues) and yellow (conserved residues). (*B*) Residues at the dimer interface of a S14:MIG12 heterodimer. S14 is shown in surface representation as in *A*. The nonconserved residues at the dimer interface, changed to the corresponding residues of MIG12 (green, shown as spheres), interact with conserved regions of S14 or are surface exposed and do not create unfavorable interactions or steric clashes. (*C*) Sequence alignment of S14 and MIG12. Conserved residues are shaded yellow, red circles denote residues at the dimer interface, and the regions of lowest homology are boxed. The secondary structure of S14 is shown below the sequence.

Blue Native PAGE studies presented here demonstrate that S14 can heterodimerize with MIG12. We have previously shown that recombinant MIG12 exists predominantly as a homodimer in solution (17) and that preformed homodimers of S14 and MIG12 are unable to associate (preliminary observations); therefore, it is likely that heterodimer formation must precede homodimerization of either S14 or MIG12.

S14 knockdown studies performed in mice show that S14 normally exists both as a S14 homodimer and as a heterodimer with MIG12. The majority of MIG12 exists as a heterodimer with S14 whereas the preponderance of S14 exists as a homodimer in mouse liver (Fig. S2). We have measured approximate concentrations of S14 and MIG12 in mouse liver using standard curves with known amounts of purified recombinant S14 and MIG12. The S14 protein concentrations in mouse liver appear to be ~10-fold higher than that of MIG12, and most MIG12 in liver normally exists as a heterodimer with S14 (preliminary observation). Heterodimer formation between S14 and MIG12 reduces MIG12's interaction with ACC, decreasing polymerization and activation of ACC, which adds another level of complexity to the regulation of ACC. Additional studies with recombinant S14:MIG12 heterodimers will be required to determine the extent to which they bind and/or change the activity of ACC.

The interaction of MIG12 with ACC1 and ACC2 is likely mediated in part by residues that are conserved between S14 and MIG12 and does not include the regions of lowest homology (box A and B, Fig. 2*C*). A limited number of amino acid substitutions might suffice to convert S14 into an ACC1 binding protein.

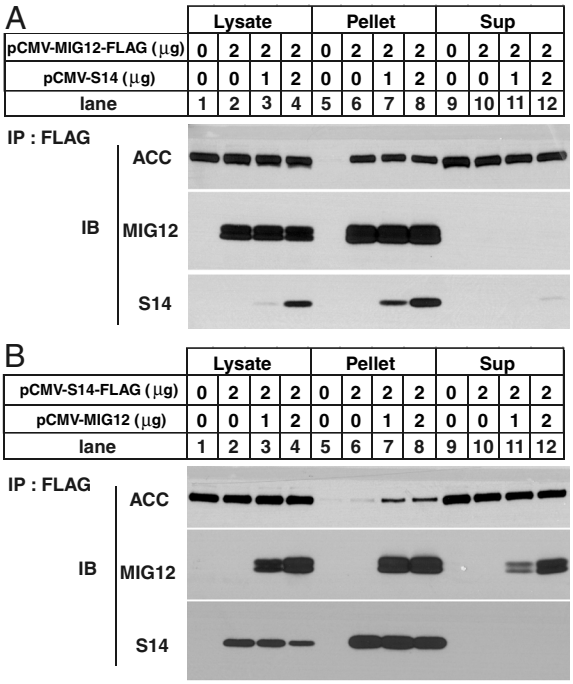

Fig. 3. Interaction of S14 and MIG12. CHO-K1 cells were transfected with the indicated amount of S14 and MIG12. (*A*) pCMV-FLAG-MIG12 and pCMV-S14 were cotransfected into CHO-K1 cells. After 24 h, cells were harvested and MIG12 was immunoprecipitated using an anti-FLAG antibody. Proteins from the whole cell lysate, pellet, and supernatant were separated by SDS-PAGE and analyzed by immunoblot using antibodies against mouse MIG12, S14, or ACC1 as described in *Materials and Methods*. (*B*) pCMV-FLAG-S14 and pCMV-MIG12 were cotransfected and analyzed as in *A*.

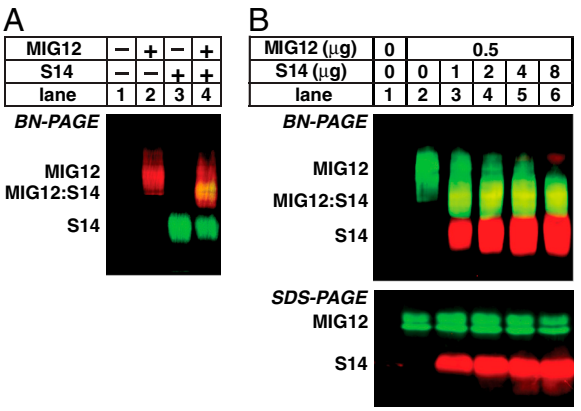

Fig. 4. S14 and MIG12 form heterodimers. (*A*) CHO-K1 cells were transfected with pCMV-MIG12 (1 μg) or pCMV-S14 (5 μg) alone, or with both plasmids. After 24 h, cells were harvested and cell lysates were prepared and separated on Blue Native PAGE (BN-PAGE) for analysis by immunoblot using rabbit polyclonal anti-MIG12 and mouse monoclonal anti-S14 antibodies. IRDye800-conjugated anti-mouse antibody and IRDye680-conjugated anti-rabbit antibody were used as the secondary antibodies. Immunoreactive bands were visualized using the LI-COR Odyssey infrared imaging system (MIG12, red; S14, green; S14:MIG12 heterodimer, yellow). (*B*) CHO-K1 cells were cotransfected with pCMV-MIG12 (0.5 μg) and the indicated amounts of pCMV-S14. After 24 h, cells were harvested and cell lysates were separated on BN-PAGE or SDS-PAGE and analyzed by immunoblot analysis as described in *A*. IRDye800-conjugated anti-rabbit antibody and IRDye680-conjugated anti-mouse antibody were used as the secondary antibodies (MIG12, green; S14, red; S14:MIG12 heterodimer, yellow).

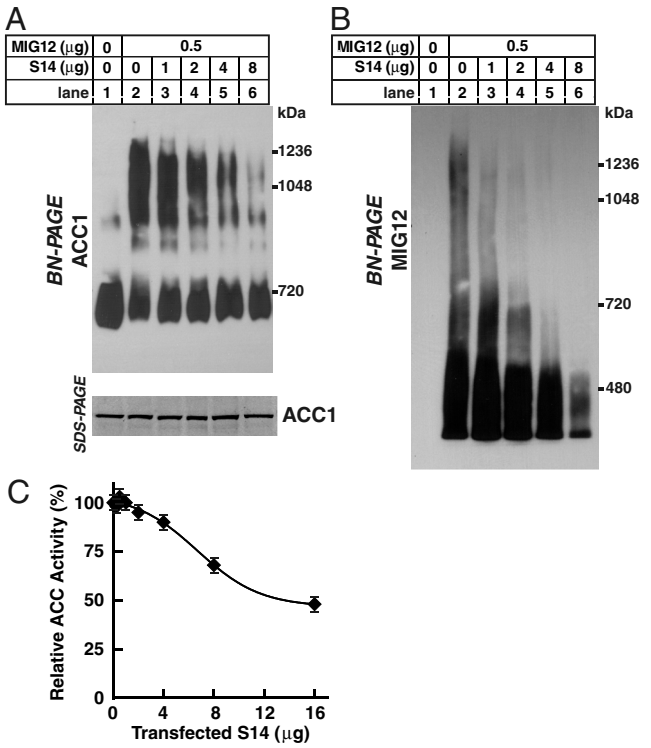

Fig. 5. S14 reduces MIG12 incorporation into ACC polymers and reduces ACC polymerization and activity. CHO-K1 cells were cotransfected with pCMV-MIG12 (0.5 μg) and the indicated amounts of pCMV-S14 (*A*–*C*). After 24 h, cells were harvested and cell lysates were prepared and separated on BN-PAGE or SDS-PAGE and analyzed by immunoblot analysis. (*A*) Cell lysates were separated by gradient BN-PAGE or SDS-PAGE and analyzed by immunoblot using a rabbit polyclonal anti-ACC1 antibody. Immunoreactive bands were visualized using LI-COR or CL-HRP substrate system. (*B*) Cell lysates were separated by gradient BN-PAGE or SDS-PAGE and analyzed by immunoblot analysis using an anti-mouse MIG12 polyclonal antibody. Immunoreactive bands were visualized using CL-HRP substrate system. (*C*) ACC activity was measured using partially purified ACC prepared from cell lysates as described in *Materials and Methods*.

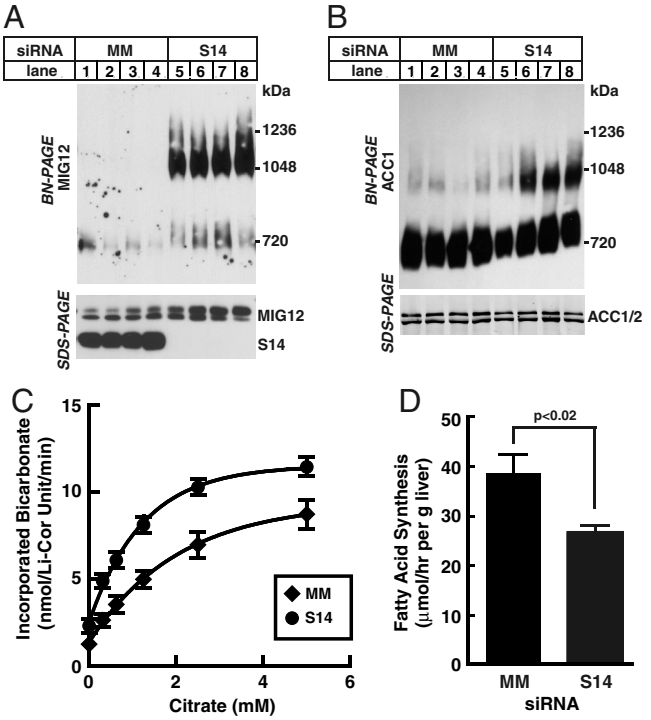

Fig. 6. Knockdown of S14 increases ACC activity in mouse liver. (*A* and *B*) Cell lysate proteins from livers of mice injected with S14 siRNA or mismatch (MM) control (four mice per group) were separated on BN-PAGE or SDS-PAGE. ACC1 and MIG12 were detected in the BN-PAGE using rabbit polyclonal anti-MIG12 (*A*) or anti-ACC1 (*B*) antibodies and the CL-HRP substrate system. ACC1/2, MIG12, and S14 proteins were detected by immunoblot analysis using IRDye680-streptavidin, rabbit polyclonal anti-MIG12, and mouse monoclonal anti-S14 antibodies. Immunoreactive bands were visualized using LI-COR. (*C*) Partially purified ACC was prepared from livers of mice injected with siRNA against S14 (●) or MM control (◆), and ACC activity was measured as described in *Materials and Methods*. ACC activity was normalized to the band intensity measured in *A*. (*D*) In vivo rates of fatty acid synthesis in livers of mice injected with MM or S14 siRNA lipidoid complexes. Five days after siRNA injections, mice were injected intraperitoneally with $[^3H]H_2O$ (50 mCi), and ^3H incorporation into newly synthesized FAs was measured as described in *Materials and Methods*. Similar results were obtained in two independent studies.

ACCs exist as dimers in solution, and the polymer is likely composed of repeating units of this dimer. MIG12 likely functions to bridge/enhance the interaction between ACC dimers resulting in increased polymerization. We have observed the presence of higher-order structures of MIG12 (17), and it is possible that these higher-order oligomers are the functional unit for enhancing activity and polymerization of ACCs. The crystallographic symmetry of the S14 crystals suggests that they might also form higher-order structures.

The tissue distribution of S14 is known to be limited to lipogenic tissues such as liver, mammary gland, and adipose tissue, whereas MIG12 is ubiquitously expressed, suggesting that S14 likely plays an important role in the regulation of fatty acid synthesis. Zhu et al. (24) reported a slight increase in hepatic fatty acid synthesis in S14 knockout mice. In contrast, Aipoalani et al. (25) showed that knockdown of S14 in rat primary hepatocytes resulted in decreased fatty acid synthesis, an effect that was further enhanced when both S14 and MIG12 were knocked down. However, the effects of the reduction in S14 on ACC activity were not measured in either of these studies.

We have previously demonstrated that S14 homodimers are unable to bind or activate ACC (17). In the current study, we have shown that regulating the levels of S14:MIG12 heterodimers regulates the ability of MIG12 to activate ACC. Increasing S14:MIG12 heterodimers by the overexpression of S14 resulted in decreased ACC activity and polymerization, whereas decreasing S14:MIG12 heterodimers by knockdown of S14 increased ACC activity and polymerization. Considering the relative amounts of S14 that exist in heterodimers with MIG12 compared to the amount of S14 that exists as a homodimer, the inhibitory effect on MIG12 may be only one function of S14 in mouse liver. Additional functions for S14 in modulating fatty acid synthesis are supported by the in vivo S14 knockdown experiments in mice that demonstrated the overall rates of fatty acid synthesis in liver are actually reduced, despite an increase in ACC activity. This is consistent with data from lactating mammary glands of S14 knockout mice in which overall fatty acid synthesis was reduced (23), despite an increase in ACC activity. Kinlaw et al. (28) reported that S14 knockdown in rat hepatocytes resulted in decreased levels of ATP-citrate lyase and an overall decrease in fatty acid synthesis, supporting the role of S14 in regulating additional proteins involved in fatty acid synthesis. Further experiments will be required to elucidate additional functions of S14 in the regulation of fatty acid synthesis.

Based upon the results presented here, we propose a model where S14 reduces the activity of MIG12 by formation of S14:MIG12 heterodimers. The S14:MIG12 heterodimers reduce the number of MIG12 homodimers that normally induce ACC polymerization and activation and/or serve a capping function preventing further polymerization and activation of ACC by MIG12. Further experiments with purified S14:MIG12

heterodimers will be required to understand the regulation of ACCs by these proteins.

Materials and Methods

Materials. [^{14}C]$KHCO_3$ (50 mCi/mmol) was obtained from American Radiolabeled Chemicals Inc. PEG 8000, acetyl-CoA sodium salt, ATP, Igepal CA-630, and $KHCO_3$ were purchased from Sigma.

Purification of S14. Mouse S14 was expressed as a GST fusion in BL21 cells (Novagen) and purified by glutathione affinity chromatography. The GST tag was removed by tobacco etch virus protease cleavage, and S14 was further purified by ion exchange followed by size exclusion chromatography. Selenomethionine containing S14 was produced in BL21 cells (29) and purified under reducing conditions.

Crystallization and Structure Determination. Crystals of S14 were formed by mixing equal volumes of S14 (10 mg/mL in 10 mM Tris pH 7.5, 50 mM NaCl, 0.01% (wt/vol) NaN_3, 1 mM DTT) with 100 mM MES pH 6.0, 15 mM $MgCl_2$, 5% (wt/vol) PEG 3000, and 30% (vol/vol) PEG 200. Cubic crystals, belonging to the space group *I*432 with unit cell dimensions of $a = b = c = 144.9$ Å, suitable for diffraction experiments, grew to dimensions of ~0.15 mm × 0.15 mm × 0.10 mm within 3 d. Selenomethionine S14 crystals were grown using similar conditions.

Crystals were transferred through a solution containing 100 mM MES pH 6.0, 15 mM $MgCl_2$, 5% (wt/vol) PEG 3000, 35% (vol/vol) PEG 200, and 20% (vol/vol) glycerol before being flash-frozen in liquid nitrogen prior to data collection at cryogenic temperature (~100 K). A two-wavelength anomalous diffraction experiment was performed on a selenomethionine derivatized crystal at the Advanced Photon Source (Argonne National Laboratory) synchrotron at the Structural Biology Center beamline 19ID. For structure solution, diffraction intensities, collected at the high-energy remote wavelength (0.9537 Å) to 2.65-Å resolution, were used in HKL3000 (30) to perform automated structure solution and initial model building.

Model Building and Refinement. Once the initial model was obtained, the model was further improved by iterations of manual model building using the program O (31) followed by refinement against a maximum likelihood target function using REFMAC5 (32). Finally, ordered solvent molecules were added to the model and the model was refined using translation libration screw-motion parameters to obtain a final $R = 22.3\%$ and $R_{free} = 24.9\%$. Additional model statistics are shown in Table 1. The refined model and structure factor amplitudes are available in the Protein Data Bank (PDB ID code 3ONT).

Immunoprecipitation. CHO K-1 cells (ATCC CCL-61) were plated at a density of 7×10^5/10-cm plate in Dulbecco's modified Eagle's medium/Ham's F-12 medium supplemented with 5% fetal calf serum, 100 units/mL penicillin G, and 100 μg/mL streptomycin sulfate on day 0. On day 2, cells were transfected with various amounts of the indicated plasmids using Fugene 6 transfection reagent (Roche). On day 3, cells were rinsed with ice cold PBS and lysed with 20 mM Hepes pH 7.6, 150 mM NaCl, 1 mM EDTA, 1% Igepal CA-630, protease inhibitors (Roche), and phosphatase inhibitors (Roche). The crude cell lysate was centrifuged at 19,000 × *g* for 20 min, and the supernatant was preincubated with 50 μL of Protein A/G agarose beads (Santa Cruz Biotechnology) for 30 min. The cleared supernatant was mixed with 50 μL of anti-FLAG M2 agarose beads (Sigma) and incubated with rotation for 2 h at 4 °C. The protein bound beads were washed 5 times with ice cold PBS supplemented with 0.05% Tween-20 and eluted with 200 μL of 100 μg/mL of FLAG peptide (Sigma) in PBS. The eluted proteins were subjected to SDS-PAGE, and immunoblot analysis was performed using anti-mouse MIG12 (17) or S14 (Roche) antibodies.

Partial Purification of ACC from Mouse Liver and CHO-K1 Cells. ACC was purified from mouse liver as described previously (17) with slight modifications. Mice were anesthetized by injecting pentobarbital (80 mg/kg), and livers were harvested by the freeze clamp method. Liver slices (0.2 g) were homogenized in 1 mL of 20 mM Hepes pH 7.6, 250 mM sucrose, 1 mM DTT, 1 mM EDTA, 1 mM EGTA, 150 mM NaF, 5 μM Compound C, protease inhibitors, and phosphatase inhibitors (Roche). The homogenate was centrifuged at 3,500 × *g* for 10 min, and the supernatant was recentrifuged at 100,000 × *g* for 45 min. Proteins in the supernatant were precipitated in 2.5% PEG 8000 at 10,000 × *g* for 15 min followed by a second round of precipitation in 5.5% PEG 8000. The pellet was washed once with distilled water and dissolved in 20 mM Hepes pH 7.6, 250 mM sucrose, 1 mM EGTA, 1 mM EDTA, 1 mM DTT, 50 mM NaF, 5 μM Compound C, and protease inhibitors.

For CHO-K1 cells, cells were washed once with 10 mL of ice cold PBS and resuspended in 400 μL of 20 mM Hepes pH 7.6, 250 mM sucrose, 1 mM DTT, 1 mM EDTA, 1 mM EGTA, 0.8 mg/mL digitonin, 150 mM NaF, 5 μM Compound C, protease inhibitors, and phosphatase inhibitors. Cell were lysed by passage through a 27-gauge needle and centrifuged at 19,000 × *g* for 20 min. Proteins in the supernatant were precipitated in 5.5% PEG 8000 at 19,000 × *g* for 5 min. The pellet was washed once with distilled water and dissolved in 20 mM Hepes pH 7.6, 250 mM sucrose, 1 mM EGTA, 1 mM EDTA, 1 mM DTT, 50 mM NaF, 5 μM Compound C, and protease inhibitors.

In Vitro ACC Activity Assay. ACC activity was measured as described previously (17).

In Vivo RNAi in Mice. siRNA oligos against mouse S14 were designed and tested for activity in cultured primary hepatocytes as described (33). The most active oligos and one containing a nucleotide mismatch for a control were synthesized and formulated into lipidoid nanoparticles as described (33) and delivered via tail vein injection (5 mg/kg body weight) into four C57BL/6J. Mice were fed a fat-free/high carbohydrate diet from the day of injection.

In Vivo Fatty Acid Synthesis in Mice. MM or S14 siRNA in lipidoid formulations were delivered via tail vein injection into 129S6/SvEv male mice at a dose of 5 mg/kg (7 mice for MM, 10 mice for S14 siRNA). Five days after siRNA administration, mice were injected intraperitoneally with ^{3}H-labeled water (50 mCi), and rates of hepatic fatty acid synthesis were determined as described (34).

Analysis of ACC Polymerization and Dimerization of S14 and MIG12 Using Blue Native Gels. Blue Native gels were prepared as described (17). Cytosolic proteins from mouse liver or CHO-K1 cells were separated using two forms of nondenaturing Blue Native PAGE: 3.5–10% for analysis of ACC and 14% for analysis of S14 and MIG12. Proteins were transferred to 0.45 μM PVDF membrane (GE Healthcare Life Sciences). Coommassie G-250 was removed from the membranes by sequential washing with methanol, water, and PBST. The membranes were incubated with blocking solution containing 5% nonfat dried milk and 5% newborn calf serum in PBST or LI-COR blocking buffer for 30 min. Immunoblot analyses were performed using rabbit polyclonal antibodies against rat ACC1, mouse MIG12 (17), and a mouse monoclonal antibody against S14 (Roche). Horseradish peroxidase linked anti-rabbit IgG (GE Healthcare) and IRDye 800-conjugated anti-rabbit antibody (LI-COR) were used as secondary antibodies to visualize ACC or MIG12. To detect S14, the membrane bound with primary antibody was incubated with biotin conjugated anti-mouse antibody (PIERCE) and then IRDye 680-conjugated streptavidin (LI-COR). Antibody bound bands were detected by Supersignal substrate system (Pierce) or LI-COR Odyssey infrared imaging system as described previously (17).

ACKNOWLEDGMENTS. We thank members of the J.D. and J.D.H. laboratories for assistance and comments during the course of this project and Chad Brautigam and Diana Tomchick for assistance with data collection. We also thank Maria Frank-Kamenetsky, Akin Akinc, Will Cantley, Victor Kotelianski, Muthiah Manoharan, Satya Kuchimanchi, Martin Maier, Rajeev Kallanthottathil, and Muthusamy Jayaraman for assistance in developing the siRNAs and formulations to S14. This work was supported in part by Welch Foundation Grant I-1185 (to J.D.), the Perot Family Foundation, and National Institutes of Health Grant HL-20948 (to J.D.H.). J.D. is an Investigator in the Howard Hughes Medical Institute. Results shown in this article are derived from work performed at Argonne National Laboratory, Structural Biology Center at the Advanced Photon Source. Argonne is operated by UChicago Argonne, LLC, for the U.S. Department of Energy, Office of Biological and Environmental Research under Contract DE-AC02-06CH11357.

1. Wakil SJ, Abu-Elheiga LA (2009) Fatty acid metabolism: Target for metabolic syndrome. *J Lipid Res* 50(Suppl):S138–143.
2. Brookheart RT, Michel CI, Schaffer JE (2009) As a matter of fat. *Cell Metab* 10:9–12.
3. Wakil SJ, Titchener EB, Gibson DM (1958) Evidence for the participation of biotin in the enzymic synthesis of fatty acids. *Biochim Biophys Acta* 29:225–226.
4. Bianchi A, et al. (1990) Identification of an isozymic form of acetyl-CoA carboxylase. *J Biol Chem* 265:1502–1509.
5. Thampy KG (1989) Formation of malonyl coenzyme A in rat heart. Identification and purification of an isozyme of A carboxylase from rat heart. *J Biol Chem* 264:17631–17634.

6. Cho YS, et al. (2008) Crystal structure of the biotin carboxylase domain of human acetyl-CoA carboxylase 2. *Proteins* 70:268–272.
7. Shen Y, Volrath SL, Weatherly SC, Elich TD, Tong L (2004) A mechanism for the potent inhibition of eukaryotic acetyl-coenzyme A carboxylase by soraphen A, a macrocyclic polyketide natural product. *Mol Cell* 16:881–891.
8. Waldrop GL, Rayment I, Holden HM (1994) Three-dimensional structure of the biotin carboxylase subunit of acetyl-CoA carboxylase. *Biochemistry* 33:10249–10256.
9. Athappilly FK, Hendrickson WA (1995) Structure of the biotinyl domain of acetyl-coenzyme A carboxylase determined by MAD phasing. *Structure* 3:1407–1419.
10. Madauss KP, et al. (2009) The human ACC2 CT-domain C-terminus is required for full functionality and has a novel twist. *Acta Crystallogr D* 65(Pt 5):449–461.
11. Zhang H, Yang Z, Shen Y, Tong L (2003) Crystal structure of the carboxyltransferase domain of acetyl-coenzyme A carboxylase. *Science* 299:2064–2067.
12. Horton JD, et al. (2003) Combined analysis of oligonucleotide microarray data from transgenic and knockout mice identifies direct SREBP target genes. *Proc Natl Acad Sci USA* 100:12027–12032.
13. Chen G, Liang G, Ou J, Goldstein JL, Brown MS (2004) Central role for liver X receptor in insulin-mediated activation of Srebp-1c transcription and stimulation of fatty acid synthesis in liver. *Proc Natl Acad Sci USA* 101:11245–11250.
14. Ishii S, Iizuka K, Miller BC, Uyeda K (2004) Carbohydrate response element binding protein directly promotes lipogenic enzyme gene transcription. *Proc Natl Acad Sci USA* 101:15597–15602.
15. Kahn BB, Alquier T, Carling D, Hardie DG (2005) AMP-activated protein kinase: ancient energy gauge provides clues to modern understanding of metabolism. *Cell Metab* 1:15–25.
16. Witters LA, Watts TD, Daniels DL, Evans JL (1988) Insulin stimulates the dephosphorylation and activation of acetyl-CoA carboxylase. *Proc Natl Acad Sci USA* 85:5473–5477.
17. Kim CW, et al. (2010) Induced polymerization of mammalian acetyl-CoA carboxylase by MIG12 provides a tertiary level of regulation of fatty acid synthesis. *Proc Natl Acad Sci USA* 107:9626–9631.
18. Seelig S, Liaw C, Towle HC, Oppenheimer JH (1981) Thyroid hormone attenuates and augments hepatic gene expression at a pretranslational level. *Proc Natl Acad Sci USA* 78:4733–4737.
19. Jump DB, Oppenheimer JH (1985) High basal expression and 3,5,3′-triiodothyronine regulation of messenger ribonucleic acid S14 in lipogenic tissues. *Endocrinology* 117:2259–2266.
20. Mater MK, Thelen AP, Pan DA, Jump DB (1999) Sterol response element-binding protein 1c (SREBP1c) is involved in the polyunsaturated fatty acid suppression of hepatic S14 gene transcription. *J Biol Chem* 274:32725–32732.
21. Ma L, Tsatsos NG, Towle HC (2005) Direct role of ChREBP.Mlx in regulating hepatic glucose-responsive genes. *J Biol Chem* 280:12019–12027.
22. Shimomura I, Shimano H, Korn BS, Bashmakov Y, Horton JD (1998) Nuclear sterol regulatory element-binding proteins activate genes responsible for the entire program of unsaturated fatty acid biosynthesis in transgenic mouse liver. *J Biol Chem* 273:35299–35306.
23. Zhu Q, et al. (2005) The Spot 14 protein is required for de novo lipid synthesis in the lactating mammary gland. *Endocrinology* 146:3343–3350.
24. Zhu Q, et al. (2001) Spot 14 gene deletion increases hepatic de novo lipogenesis. *Endocrinology* 142:4363–4370.
25. Aipoalani DL, O'Callaghan BL, Mashek DG, Mariash CN, Towle HC (2010) Overlapping roles of the glucose-responsive genes, S14 and S14R, in hepatic lipogenesis. *Endocrinology* 151:2071–2077.
26. Chou WY, et al. (2007) Human spot 14 protein interacts physically and functionally with the thyroid receptor. *Biochem Biophys Res Commun* 357:133–138.
27. Cunningham BA, Maloney M, Kinlaw WB (1997) Spot 14 protein-protein interactions: Evidence for both homo- and heterodimer formation in vivo. *Endocrinology* 138:5184–5188.
28. Kinlaw WB, Church JL, Harmon J, Mariash CN (1995) Direct evidence for a role of the "spot 14" protein in the regulation of lipid synthesis. *J Biol Chem* 270:16615–16618.
29. Doublie S (1997) Preparation of selenomethionyl proteins for phase determination. *Methods Enzymol* 276:523–530.
30. Otwinowski Z, Minor W (1997) Processing of x-ray diffraction data collected in oscillation mode. *Meth Enzymol* 276:307–326.
31. Jones TA, Zou JY, Cowan SW, Kjeldgaard M (1991) Improved methods for building protein models in electron density maps and the location of errors in these models. *Acta Crystallogr A* 47(Pt 2):110–119.
32. Murshudov GN, Vagin AA, Dodson EJ (1997) Refinement of macromolecular structures by the maximum-likelihood method. *Acta Crystallogr D* 53(Pt 3):240–255.
33. Frank-Kamenetsky M, et al. (2008) Therapeutic RNAi targeting PCSK9 acutely lowers plasma cholesterol in rodents and LDL cholesterol in nonhuman primates. *Proc Natl Acad Sci USA* 105:11915–11920.
34. Shimano H, et al. (1996) Overproduction of cholesterol and fatty acids causes massive liver enlargement in transgenic mice expressing truncated SREBP-1a. *J Clin Invest* 98:1575–1584.